

Molten Salt Synthesis of Bi_2WO_6 Powders and its Visible-Light Photocatalytic Activity

Bing Dai^{a,b}, Ming Xuan^{a,b}, Yaohui Lv^c, Chuangui Jin^{c*}, Songlin Ran^{a,b}

^aKey Laboratory of Metallurgical Emission Reduction & Resources Recycling (Anhui University of Technology), Maanshan, P. R. China

^bAnhui Province Key Laboratory of Metallurgy Engineering & Resources Recycling (Anhui University of Technology), Maanshan, P. R. China

^cSchool of Materials Science and Engineering, Anhui University of Technology, Maanshan, P. R. China

Received: April 29, 2019; Revised: July 24, 2019; Accepted: August 25, 2019

Bi_2WO_6 powders were synthesized by the molten salt method at 250–350 °C using the mixture of $\text{Bi}(\text{NO}_3)_3 \cdot 5\text{H}_2\text{O}$ and $\text{Na}_2\text{WO}_4 \cdot 2\text{H}_2\text{O}$ as a precursor, and the mixture of LiNO_3 and NaNO_3 with a molar ratio of 27:33 as a molten salt, respectively. The effects of temperature and salt amount on the phase composition, morphology and photocatalytic activity under the visible light irradiation were investigated. The results revealed that pure phase Bi_2WO_6 powders could be synthesized at 350 °C as the weight of molten salts were 2–5 times as many as the precursor. Bi_2WO_6 powder synthesized with lower salt amount exhibited larger surface area, more abundant pores, narrower bandgap and lower PL intensity, all of which contributed a higher photocatalytic activity. The synthesized Bi_2WO_6 powder could degrade 0.01 mol/L Rhodamine-B solution by 97% after irradiation under visible light for 60 min. The obtained Bi_2WO_6 powder had a good photochemical stability and reusability, revealing potential application in environmental treatment.

Keywords: Bi_2WO_6 , Molten salt method, Photocatalysis, Environmental treatment.

1. Introduction

Environmental pollution is one of the most important problems for the mankind. Photocatalytic oxidation & reduction method has attracted much attention due to its low energy consumption and low pollution in environmental treatment¹. As a typical photocatalyst, TiO_2 has been commercialized and widely applied in the fields of organic degradation, environmental cleaning and sterilization, heavy metal pollution control and so on². However, due to its wide band gap, TiO_2 is only be driven by the ultraviolet light which only takes up no more than 5% of the total solar energy impinging on the surface of the earth. Therefore, in view of full solar light utilization, it is still of great importance and challenge to explore new photocatalysts which could be driven by not only the ultraviolet light, but also the visible light and the near-infrared light^{3,4}.

Among various new photocatalysts, bismuth tungstate (Bi_2WO_6) with an orthorhombic structure has attracted considerable attentions^{5–12}. Bi_2WO_6 is constructed by alternating $(\text{Bi}_2\text{O}_2)_n^{2n+}$ layers and perovskite-like $(\text{WO}_4)_n^{2n-}$ layers with a relatively narrow band gap of about 2.8 eV⁹. Researches have demonstrated that Bi_2WO_6 exhibited excellent photocatalytic properties under the irradiation of both visible light and the near-infrared light^{6–8}. Traditionally, Bi_2WO_6 powders were prepared by solid-state reaction and hydrothermal method. The solid-state reaction was the simplest synthesis method for obtaining Bi_2WO_6 powders but the synthesis temperature was as high as 900 °C, which resulted in small surface area and poor photocatalytic performance of the product¹³.

Bi_2WO_6 powders with large surface area could be synthesized by the hydrothermal method at low temperature (120–250 °C) but the synthesis process was limited in special autoclaves^{5,14}. In addition, surfactants were usually indispensable in order to keep the Bi_2WO_6 particles with monodisperse or induce the crystal growth of Bi_2WO_6 into special morphologies⁵.

As a powder synthesis method, molten salt method is as simple as solid-state reaction but with much faster mass transfer transport by providing liquid circumstance. Various molten salt systems have been used as reaction media for the powder synthesis and crystal growth of different ceramic and metal powders^{15,16}. In addition, the use of water-soluble salts can make the separation of products very easy. Compared to solid state reaction, the molten salt method can synthesize powders at lower temperature with finer particle size and/or more special morphology. Recently, our group reported the synthesis of Bi_2WO_6 powders by a molten salt method using precipitate, from mixed $\text{Bi}(\text{NO}_3)_3$ and Na_2WO_4 aqueous solutions with addition of ammonia, as precursors¹⁷. The results indicated that pure phase Bi_2WO_6 powders could be obtained at 250–350 °C. The addition of molten salt greatly enhanced the surface area of the powders and induced a plate-like morphology. In this paper, for the purpose of simplifying the synthesis process, Bi_2WO_6 powders were synthesized by the molten salt method directly with solid $\text{Bi}(\text{NO}_3)_3$ and Na_2WO_4 as precursors. The effects of calcination temperature, soaking time and salt amount on the phase composition, morphology and the photocatalytic activity of the synthesized powders were investigated.

* e-mail: jcg@ahut.edu.cn

2. Experimental Procedure

Commercial $\text{Bi}(\text{NO}_3)_3 \cdot 5\text{H}_2\text{O}$, $\text{Na}_2\text{WO}_4 \cdot 2\text{H}_2\text{O}$, LiNO_3 and NaNO_3 were used as raw materials. All of the above chemicals were analytical grade and purchased from Sinopharm Chemical Reagent Co., Ltd. in China. In a typical synthesis process, $\text{Bi}(\text{NO}_3)_3 \cdot 5\text{H}_2\text{O}$ and $\text{Na}_2\text{WO}_4 \cdot 2\text{H}_2\text{O}$ with an atomic molar ratio of Bi/W of 2:1 were firstly mixed by hand in an agate mortar with a pestle for 10 min. Then, LiNO_3 and NaNO_3 with a molar ratio of 27:23 were mixed with the same method for 10 min. The mixture of $\text{LiNO}_3/\text{NaNO}_3$ has lower melting point (194 °C) than either LiNO_3 (264 °C) or NaNO_3 (307 °C), which could provide liquid circumstance earlier to accelerate the reaction process. The two mixtures were mixed together for another 10 min and were placed into a corundum crucible. The crucible was put into an electric resistance furnace and heated at 250–350 °C for 8 h with a heating rate of 10 °C/min. Subsequently, the crucible was cooled naturally to room temperature. After immersed in distilled water to dissolve nitrates, the precipitate was filtered, washed using distilled water for several times and absolute ethanol for the last time, respectively. Finally, the powders were dried at 80 °C overnight.

The crystalline phase compositions of the samples were identified using X-ray diffraction (XRD, Ultima IV, Rigaku, Japan) with a Cu-K α radiation ($\lambda=1.54178 \text{ \AA}$). The microstructures of the samples were characterized using field-emission scanning electron microscope (FE-SEM, Nova NanoSEM, NPE207, FEI, USA). The specific surface area was measured by the Brunauer-Emmett-Teller (BET) method using a nitrogen absorption analysis (Tri-star 3000, Micromeritics Instrument Corp., USA). The UV-Vis diffuse reflectance spectra (DRS) was recorded using an UV-Vis spectrophotometer (UV-3600, Shimadzu, Japan). The photoluminescence (PL) spectra of the synthesized powders were carried out on a Hitachi F-4600 fluorescence spectrophotometer.

The photocatalytic activities of the samples were assessed by the photodegradation of Rhodamine-B (RhB) under the irradiation of visible light. In a typical process, 250 mL RhB solution with a concentration of 0.01 mmol/L was put into a quartz reactor. 0.25 mg synthesized powders were added and stirred magnetically in the dark for 30 min. After the adsorption-desorption equilibrium between the powders and RhB was established, the solution was irradiated by the visible light with a 500 W Xe lamp ($\lambda > 420 \text{ nm}$) under continuous stirring. The solution with a volume of 4 mL was extracted using a syringe at an interval of 30 min. After centrifugal separation, the clear solution was analyzed on a UV-Vis spectrophotometer (UV-2102PC, Beijing Purkinje General Instrument Co., Ltd., China) at a wavelength of 554 nm. The photocatalytic efficiency was calculated by the value of C/C_0 , where C_0 and C was the concentration of the starting RhB solution and the RhB solution after photocatalytic test for a certain time, respectively.

3. Results and Discussion

Bi_2WO_6 powders were synthesized by heat treating the precursor in the salt bath. The effects of temperature and salt amount on the phase composition of the obtained product were investigated. Fig. 1 shows the XRD patterns of samples synthesized at 250–350 °C with a mass ratio of 5:1 for the salt and the precursor. When the temperature is 250 °C, the target phase Bi_2WO_6 (JCPDS 39-0256) is the main crystalline phase, as shown in Fig. 1a. However, there is still other peaks belong to $\text{Bi}_{14}\text{W}_2\text{O}_{27}$, WO_3 and unknown phases. The XRD peaks for Bi_2WO_6 phase are wide with low intensity, which indicates that the crystallinity of Bi_2WO_6 phase is still low. Normally, increasing temperature is used to improve the reaction process and enhance the crystallinity of the product. As a result, the synthesis temperature was increased to 300 °C. According to Fig. 1b, the increase of temperature greatly decreases the amount of impurities which only have trace peaks in the XRD pattern. In the meantime, the XRD peaks for Bi_2WO_6 phase are becoming narrower and stronger (Fig. 1b). As the temperature increases to 350 °C, Bi_2WO_6 phase has already been the only crystalline phase in the sample and no other impurity peaks are observed from the XRD pattern in Fig. 1c. The above results reveals that pure Bi_2WO_6 powders could be successfully synthesized by the molten salt method directly using the mixture of $\text{Bi}(\text{NO}_3)_3 \cdot 5\text{H}_2\text{O}$ and $\text{Na}_2\text{WO}_4 \cdot 2\text{H}_2\text{O}$ as a precursor.

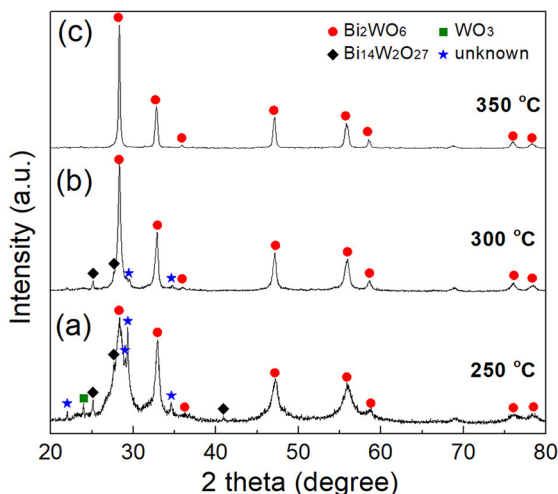


Figure 1. XRD patterns of samples synthesized at different temperatures with a mass ratio of 5:1 for the salt and the precursor.

Fig. 2 shows the XRD patterns of samples synthesized at 350 °C with different mass ratio of the salt and the precursor. Without the addition of $\text{LiNO}_3/\text{NaNO}_3$ salt, impurities such as $\text{Na}_2\text{W}_4\text{O}_{13}$ and Bi_2O_3 appear in the XRD pattern (see Fig. 2a). When the salt is added, the impurities disappear in Fig. 2b and Fig. 2c, revealing that the liquid atmosphere accelerated the mass transport of the reactants.

However, too much salt made it difficult for the reactants to contact each other and decelerate the mass transport¹⁸, which resulted in unknown impurities, as indicated in Fig. 2d. In our previous report¹⁷, Bi_2WO_6 powders were synthesized by the same molten salt method using the same salts but with precipitates from mixed $\text{Bi}(\text{NO}_3)_3$ and Na_2WO_4 aqueous solutions with addition of ammonia as precursors, and pure crystallized Bi_2WO_6 powders could be obtained at a temperature as low as 250 °C. The different minimum temperature for the pure product indicates that the precursor is one of the key factors in the molten salt method.

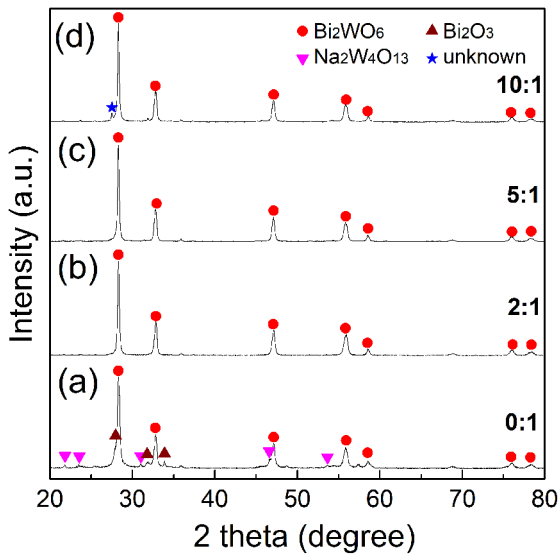


Figure 2. XRD patterns of samples synthesized at 350 °C with different mass ratio of the salt and the precursor.

The morphologies of the synthesized pure Bi_2WO_6 powders were observed by SEM (Fig. 3). It was found that the salt amount greatly affected the morphology of the as-synthesized powders. When the salt amount was low, the obtained powders showed a plate-like shape with a thickness less than 50 nm, as shown in Fig. 3a. When the salt amount was high, the prepared powders had a columnar morphology,

as illustrated in Fig. 3b. In our previous research¹⁷, Bi_2WO_6 powders with the same morphology were synthesized by the same molten salt method with a different precursor. Like this study, the morphology could be controlled by the salt amount, and the powders with a plate-like shape exhibited much higher photocatalytic activity than those with a particle-like morphology¹⁷.

Fig. 4 shows the nitrogen adsorption and desorption isotherms of the synthesized Bi_2WO_6 powders. Both samples show a type H3 hysteresis loop¹⁹, which does not exhibit any limiting adsorption at high P/P_0 , indicating the presence of slit-shaped pores¹⁹. The pore size distribution of the samples, as shown in the inset of Fig. 4, depends on the salt amount. When lower salt amount was used, the peaks around 20 nm and 40 nm are much stronger, revealing more pores in the prepared powders. The measured BET surface area of the samples was 8.77 $\text{m}^2 \text{g}^{-1}$ and 8.16 $\text{m}^2 \text{g}^{-1}$ for the powders synthesized with low and high salt amount, respectively. The values are much lower than those (12.93–21.86 $\text{m}^2 \text{g}^{-1}$) in our previous report, but a little higher than that (7.08 $\text{m}^2 \text{g}^{-1}$) for the Bi_2WO_6 powders synthesized from calcining precipitate precursor without the present of molten salts¹⁷.

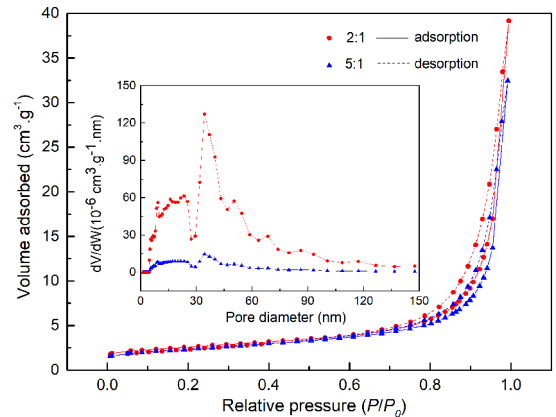


Figure 4. Nitrogen sorption isotherms and pore size distributions of samples synthesized with different salt amount.

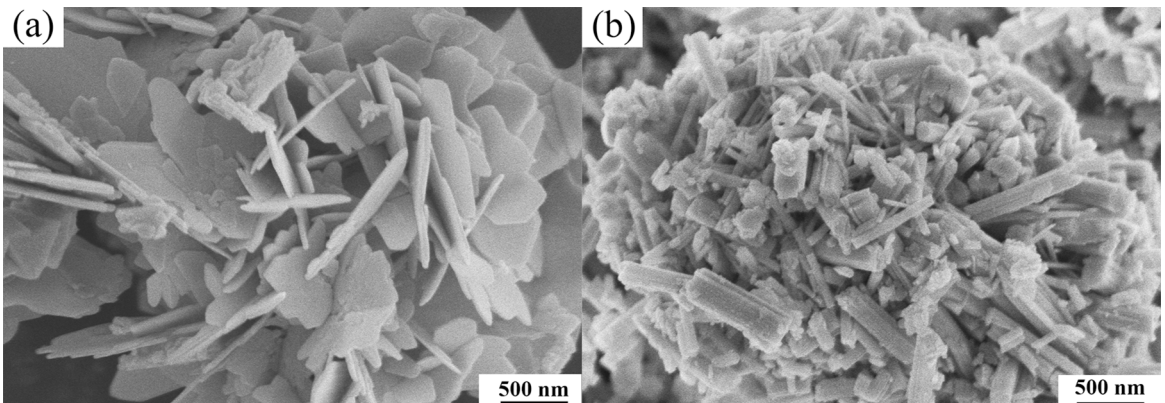


Figure 3. SEM images of samples synthesized at 350 °C with a mass ratio of (a) 2:1 and (b) 5:1 for the salt and the precursor.

The difference in the porosity and BET surface area would affect the photocatalytic properties of the corresponding samples. Large surface area increases reactive sites and promotes electron-hole separation efficiency²⁰. The presence of pores allows the penetration of light waves and organic molecules in solution deep into the photocatalyst²¹. Bi₂WO₆ powder synthesized with lower salt amount was expected to perform better in photodegradation test due to its larger surface area and more abundant pores.

The optical absorption properties of the synthesized pure Bi₂WO₆ powders were investigated by performing UV-Vis tests. As shown in Fig. 5, both powders present nearly the same optical absorption at a wavelength between 200 nm and 800 nm. Moreover, both absorption curves have sharp edges in the visible light region around 450 nm, revealing that the visible light absorption is caused by a band-gap transition rather than a transition from an impurity level. As a crystalline semiconductor, the optical absorption near the band edge complies with the Kubelka-Munk equation²².

$$\alpha hv = A(hv - E_g)^n \quad (1)$$

Where α -absorption coefficient; h -Planck's constant; ν -light frequency; E_g -forbidden bandgap; A -constant (usually 1); n -decided by the optical transition type of typical semiconductors. According to previous reports¹⁷, the value of n is 2 for Bi₂WO₆. The bandgap of the Bi₂WO₆ could be estimated from tangent lines in the plots of the square root of the Kubelka-Munk functions ($(\alpha hv)^{1/2}$) against the photon energy ($h\nu$), as shown in the inset of Fig. 5. Considering considerable absorbance at energies below the bandgap, the baseline was subtracted by fitting an appropriate straight line to the functions before the slope appeared²³. The bandgap was calculated as 2.76 eV and 2.78 eV for the powders synthesized with low and high salt amount, respectively, which are higher than those (2.64–2.68 eV) in our previous report¹⁷. The results revealed that both samples have a bandgap suitable for photocatalytic degradation of organic contaminants under visible light irradiation.

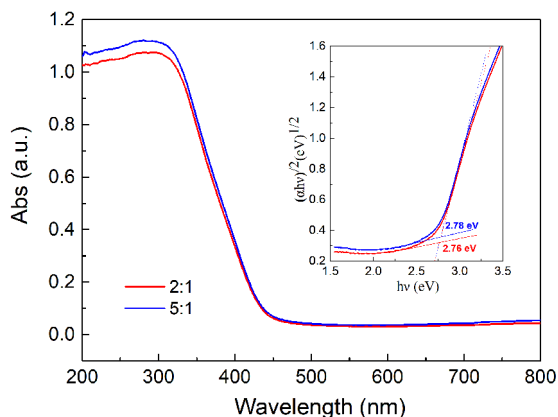


Figure 5. UV-Vis diffuse reflectance spectra of samples synthesized with different salt amount.

The bandgap of Bi₂WO₆ powders prepared with lower salt amount is narrower, which is benefit to its photocatalytic performance.

Fig. 6 shows the PL spectra of Bi₂WO₆ powder synthesized with different salt amount. It is clear that Bi₂WO₆ powder from lower salt amount achieves lower PL intensity, suggesting that decreasing salt amount can enhance the separation efficiency of photo-generated electrons and holes. As a result, Bi₂WO₆ powder synthesized with lower salt amount would exhibit enhanced photocatalytic activity.

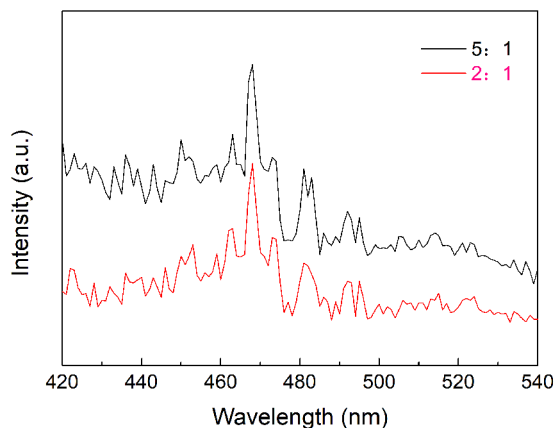


Figure 6. PL spectra of samples synthesized with different salt amount.

In order to evaluate the effect of salt amount on the photocatalytic activity of the synthesized Bi₂WO₆ powders, the photocatalytic degradation of RhB dye was performed under visible light ($\lambda > 420$ nm). The test result is shown in Fig. 7. It can be seen from Fig. 7a that there is nearly no change of RhB concentration under the irradiation of the visible light without photocatalyst. When the synthesized Bi₂WO₆ powders were added, the RhB concentration continuously decreased with increasing irradiation time, indicating photocatalytic activity of the products under visible light. It is clear that the Bi₂WO₆ powders synthesized with lower salt amount exhibited much higher photocatalytic activity. When using the Bi₂WO₆ powders synthesized with low salt amount as a photocatalyst, 97% RhB was degraded in 60 min. However, when the Bi₂WO₆ powders synthesized with high salt amount was used as a photocatalyst, only 55% RhB could be degraded in 60 min.

Fig. 7b shows the linear fitting of $\ln(C/C_0)$ and irradiation time for the RhB solution photodegraded by Bi₂WO₆ synthesized with different salt amount. The reaction kinetics of the RhB solution between the two catalyst powders were compared, assuming a first-order reaction kinetics model i.e. $\ln(C/C_0) = -kt$, where C_0 and C are the concentrations of RhB after absorption-desorption equilibrium and photocatalytic test for a certain time, respectively. The pseudo first-order kinetic (k) values was calculated to be 0.039 min⁻¹ for the Bi₂WO₆ powder synthesized with lower salt amount and 0.014 min⁻¹ for that with higher salt amount, respectively.

The different k values indicated that the salt amount using in the synthesis process greatly affected the photocatalytic activity of the obtained photocatalyst.

Fig. 7c illustrates the UV-vis spectra of RhB solution at different irradiation times using Bi_2WO_6 powder synthesized with lower salt amount as a photocatalyst. During the photodegradation process, the absorption of RhB was gradually reduced at the wavelength of 554 nm, accompanied with an absorption band hypsochromic shift. After 90 min of irradiation, there was almost no absorption, which was consistent with the photocatalytic degradation curve in Fig. 7a. The UV-vis spectra changes of RhB solution during the photodegradation process in this study are similar to the literatures^{14,17,24}. In this study, the light wavelength was longer than 420 nm, and the photodegradation of RhB in this range includes the photocatalytic process and the photosensitized process. Previous report has demonstrated that the photocatalytic process was the predominant process when RhB solution was photodegraded by Bi_2WO_6 catalyst²⁵. As the Bi_2WO_6 powder absorbs visible light ($\lambda < 472$ nm), the electrons transition from the valence band to conduction band generate photogenerated electrons and holes. The released electrons react with oxygen molecules to generate another active species superoxide radical ($\cdot\text{O}_2^-$). Both the photogenerated holes and $\cdot\text{O}_2^-$ have strong oxidizing potential which could degrade the dye by oxidation reactions²⁶. Sometimes, for

example, there is monolayer or oxygen-deficient for Bi_2WO_6 powder, hydroxyl radicals ($\cdot\text{OH}$) could also be generated^{5,27}, which is greatly beneficial for the photocatalytic reaction.

According to previous discussion, there is differences between the two powders in particle morphology (Fig. 3), specific surface area, pore size distribution (Fig. 4), optical absorption (Fig. 5) and PL properties (Fig. 6). Bi_2WO_6 powder synthesized with lower salt amount has larger surface area, more abundant pores, narrower bandgap and lower PL intensity, all of which contribute a higher photocatalytic activity. Compared with our previous report¹⁷, the Bi_2WO_6 powders synthesized in this study exhibited worse photocatalytic activities due to their much lower specific surface area and bandgaps. However, the precursor used in this study is simple, which is benefit for the powder production for commercial applications.

The photochemical stability and reusability of the Bi_2WO_6 catalyst synthesized with lower salt amount was evaluated by cyclic experiments and XRD, as shown in Fig. 8. After the photocatalytic reaction for 5 cycles, the photocatalytic activity of the photocatalyst slightly decreased at the first 30 min illumination, and tended to be the same with increasing illumination time (Fig. 8a). The same XRD patterns in Fig. 8b means that the cyclic experiments had no effect on the crystal structure of the Bi_2WO_6 catalyst. The above results indicate that the synthesized Bi_2WO_6 powders have good photochemical stability and reusability, which is beneficial for potential application.

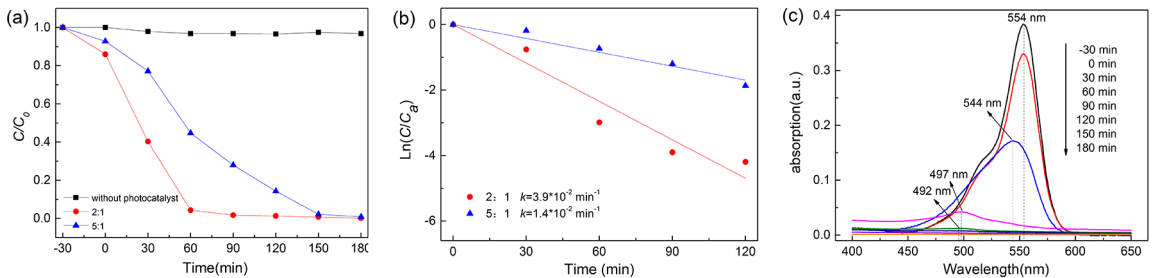


Figure 7. (a) Photocatalytic degradation curves and (b) the linear fitting of $\ln(C/C_0)$ and irradiation time for the RhB solution photodegraded by Bi_2WO_6 synthesized with different salt amount, (c) UV-vis spectra of RhB at different irradiation times with Bi_2WO_6 synthesized with lower salt amount as a photocatalyst.

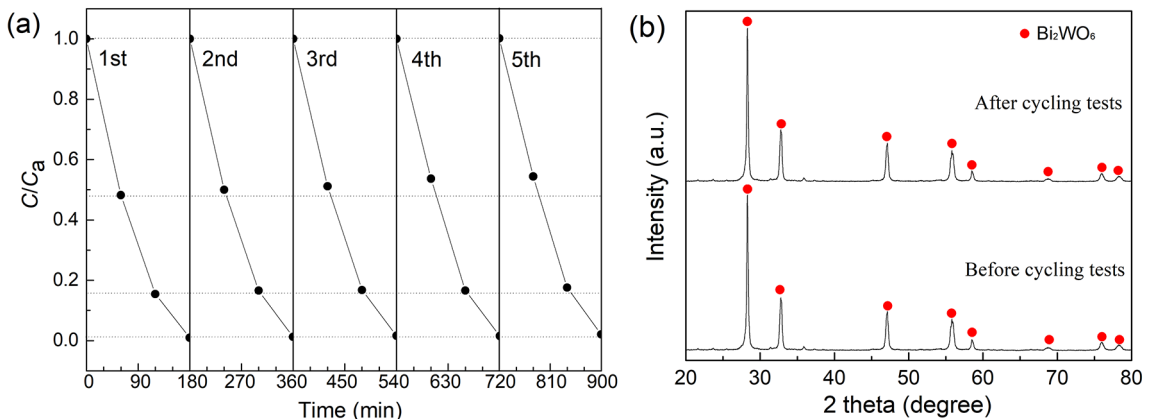


Figure 8. (a) Cycling test for the photocatalytic degradation of RhB, (b) XRD patterns of Bi_2WO_6 powders before and after 5 times cycling tests.

4. Conclusions

Bi_2WO_6 photocatalytic powders were successfully synthesized by calcining the mixture of chemical reagent $\text{Bi}(\text{NO}_3)_3 \cdot 5\text{H}_2\text{O}$ and $\text{Na}_2\text{WO}_4 \cdot 2\text{H}_2\text{O}$ in molten $\text{LiNO}_3/\text{NaNO}_3$ salt bath. The results indicated that the synthesis temperature and the salt amount greatly affected the phase composition of the products. The addition of appropriate amount of $\text{LiNO}_3/\text{NaNO}_3$ introduced a liquid circumstance for the reaction, which improved the substances diffusion and thus accelerated the reaction. The salt amount using in the synthesis process greatly affected the morphology, the pore distribution, bandgap and PL intensity of the obtained Bi_2WO_6 powder. Lower salt amount induced a higher photocatalytic activity in degradation of RhB. When the weight of $\text{LiNO}_3/\text{NaNO}_3$ salt was 2 times as many as $\text{Bi}(\text{NO}_3)_3 \cdot 5\text{H}_2\text{O}/\text{Na}_2\text{WO}_4 \cdot 2\text{H}_2\text{O}$ precursor, the as-synthesized Bi_2WO_6 powders at 350 °C exhibited the highest degradation efficiency under the visible light irradiation, which could completely bleach 10^{-5} mol/L RhB solution effectively and the removal efficiency was 97 % in 60 min. The synthesized Bi_2WO_6 powder also showed a good photochemical stability and reusability.

5. Acknowledgements

This work was supported by the National Natural Science Foundation of China (U1860102) and Anhui Provincial Natural Science Foundation (1808085ME138).

6. References

- Li X, Xie J, Jiang C, Yu J, Zhang P. Review on design and evaluation of environmental photocatalysts. *Frontiers of Environmental Science & Engineering*. 2018;12(5):14.
- Dong B, Liu T, Li C, Zhang F. Species, engineering and characterizations of defects in TiO_2 -based photocatalyst. *Chinese Chemical Letters*. 2018;29(5):671-680.
- Tong H, Ouyang S, Bi Y, Umezawa N, Oshikiri M, Ye J. Nanophotocatalytic materials: possibilities and challenges. *Advanced Materials*. 2012 Jan;24(2):229-51.
- Sang Y, Liu H, Umar A. Photocatalysis from UV/Vis to near-infrared light: Towards full solar-light spectrum activity. *ChemCatChem*. 2015 Feb;7(4):559-573.
- Zhou Y, Zhang Y, Lin M, Long J, Zhang Z, Lin H, Wu JC-S, Wang X. Monolayered Bi_2WO_6 nanosheets mimicking heterojunction interface with open surfaces for photocatalysis. *Nature communications*. 2015;6:8340.
- Zhang G, Hu Z, Sun M, Liu Y, Liu L, Liu H, Huang CP, Qu J, Li J. Formation of Bi_2WO_6 bipyramids with vacancy pairs for enhanced solar-driven photoactivity. *Advanced Functional Materials*. 2015 Jun;25(24):3726-3734.
- Lv Y, Yao WQ, Zong R, Zhu Y. Fabrication of wide-range-visible photocatalyst $\text{Bi}_2\text{WO}_{6-x}$ nanoplates via surface oxygen vacancies. *Scientific Reports*. 2016 Jan;6:19347.
- Tian J, Sang Y, Yu G, Jiang H, Mu X, Liu H. A Bi_2WO_6 -based hybrid photocatalyst with broad spectrum photocatalytic properties under UV, visible, and near-infrared irradiation. *Advanced Materials*. 2013 Jul;25(36):5075-5080.
- Kumar SG, Rao KSRK. Tungsten-based nanomaterials (WO_3 & Bi_2WO_6): Modifications related to charge carrier transfer mechanisms and photocatalytic applications. *Applied Surface Science*. 2015;355:939-958.
- Zhang N, Ciriminna R, Pagliaro M, Xu YJ. Nanochemistry-derived Bi_2WO_6 nanostructures: Towards production of sustainable chemicals and fuels induced by visible light. *Chemical Society Reviews*. 2014 Aug;43(15):5276-5287.
- Zhang L, Zhu Y. A review of controllable synthesis and enhancement of performances of bismuth tungstate visible-light-driven photocatalysts. *Catalysis Science & Technology*. 2012 Apr;2(4):694-706.
- He R, Cao S, Peng Z, Yu J. Recent advances in visible light Bi-based photocatalysts. *Chinese Journal of Catalysis*. 2014 Jul;35(7):989-1007.
- Tang J, Zou Z, Ye J. Photocatalytic decomposition of organic contaminants by Bi_2WO_6 under visible light irradiation. *Catalysis Letters*. 2004 Jan;92(1-2):53-56.
- Zhou YX, Tong L, Zeng XH, Chen XB. Green synthesis of flower-like Bi_2WO_6 microspheres as a visible-light-driven photocatalyst. *New Journal of Chemistry*. 2014 May;38(5):1973-1979.
- Liu X, Fechner N, Antonietti M. Salt melt synthesis of ceramics, semiconductors and carbon nanostructures. *Chemical Society Reviews*. 2013 Nov;42(21):8237-65.
- Zhang H, Dasbiswas K, Ludwig NB, Han G, Lee B, Vaikuntanathan S, Talapin DV. Stable colloids in molten inorganic salts. *Nature*. 2017 Feb;542(7641):328-331.
- Zhou L, Jin C, Yu Y, Chi F, Ran S, Lv Y. Molten salt synthesis of Bi_2WO_6 powders with enhanced visible-light-induced photocatalytic activities. *Journal of Alloys and Compounds*. 2016 Apr;680(25):301-308.
- Liu Z, Wei Y, Meng X, Wei T, Ran S. Synthesis of CrB_2 powders at 800 °C under ambient pressure. *Ceramics International*. 2017;43(1 Pt B):1628-1631.
- Sing KSW, Everett DH, Haul RAW, Moscou L, Pierotti RA, Rouquérol J, Siemieniowska T. Reporting physisorption data for gas/solid systems with special reference to the determination of surface area and porosity. *Pure and Applied Chemistry*. 1985;57(4):603-619.
- Yu J, Xiong J, Cheng B, Liu S. Fabrication and characterization of Ag-TiO₂ multiphase nanocomposite thin films with enhanced photocatalytic activity. *Applied Catalysis B Environmental*. 2005 Oct;60(3-4):211-221.
- Xu X, Ge Y, Wang H, Li B, Yu L, Liang Y, Chen K, Wang F. Sol-gel synthesis and enhanced photocatalytic activity of doped bismuth tungsten oxide composite. *Materials Research Bulletin*. 2016 Jan;73:385-393.
- Butler M. Photoelectrolysis and physical properties of the semiconducting electrode WO_2 . *Journal of Applied Physics*. 1977;48(5):1914-1920.

23. Makuła P, Pacia M, Macyk W. How to correctly determine the band gap energy of modified semiconductor photocatalysts based on UV–Vis spectra. *The Journal of Physical Chemistry Letters*. 2018 Dec;9(23):6814-6817.
24. Huang H, Liu K, Chen K, Zhang Y, Zhang Y, Wang S. Ce and F comodification on the crystal structure and enhanced photocatalytic activity of Bi_2WO_6 photocatalyst under visible light irradiation. *The Journal of Physical Chemistry C*. 2014;118(26):14379-14387.
25. Fu H, Pan C, Yao W, Zhu Y. Visible-light-induced degradation of rhodamine B by nanosized Bi_2WO_6 . *The Journal of Physical Chemistry B*. 2005 Dec;109(47):22432-9.
26. Fu H, Zhang S, Xu T, Zhu Y, Chen J. Photocatalytic degradation of RhB by fluorinated Bi_2WO_6 and distributions of the intermediate products. *Environmental Science & Technology*. 2008 Mar;42(6):2085-91.
27. Yang L, Bo W, Xu L, Hong G, Zhang M. Generation of oxygen vacancy and oh radicals: A comparative study of Bi_2WO_6 and $\text{Bi}_2\text{WO}_{6-x}$ nanoplates. *ChemCatChem*. 2015 Oct;7(24):4076-4084.